Letter

Strong effects of uniaxial pressure and short-range correlations in $Cr_2Ge_2Te_6$

S. Spachmann [1,*] A. Elghandour [1] S. Selter [2] B. Büchner [2,3] S. Aswartham [2,†] and R. Klingeler [1,‡]

[1] *Kirchhoff Institute for Physics, Heidelberg University, INF 227, 69120 Heidelberg, Germany*

[2] *Leibniz Institute for Solid State and Materials Research (IFW), Helmholtzstraße 20, 01069 Dresden, Germany*

[3] *Institute of Solid State and Materials Physics and Würzburg-Dresden Cluster of Excellence ct.qmat, Technische Universität Dresden, 01062 Dresden, Germany*

(Received 7 February 2022; revised 11 April 2022; accepted 25 April 2022; published 20 May 2022)

$Cr_2Ge_2Te_6$ is a quasi-two-dimensional semiconducting van der Waals ferromagnet down to the bilayer with great potential for technological applications. Engineering the critical temperature to achieve room-temperature applications is one of the critical next steps on this path. Here, we report high-resolution capacitance dilatometry studies on $Cr_2Ge_2Te_6$ single crystals which directly prove significant magnetoelastic coupling and provide quantitative values of the large uniaxial pressure effects on long-range magnetic order ($\partial T_C/\partial p_c = 24.7$ K/GPa and $\partial T_C/\partial p_{ab} = -15.6$ K/GPa) derived from thermodynamic relations. Moderate in-plane strain is thus sufficient to strongly enhance ferromagnetism in $Cr_2Ge_2Te_6$ up to room temperature. Moreover, unambiguous signs of short-range magnetic order up to 200 K are found.

DOI: 10.1103/PhysRevResearch.4.L022040

Strain is a versatile parameter to engineer electronic, optical, thermal, or chemical properties of materials in semiconductor technology [1–5]. When technologically relevant phenomena in unstrained single crystals or epitaxial films appear only at low temperatures, it can be used particularly to tune the relevant phenomena toward room temperature [6–8]. The quasi-two-dimensional (quasi-2D) van der Waals (vdW) semiconducting ferromagnet $Cr_2Ge_2Te_6$ is such an example of great potential for technological applications as it shows ferromagnetism in bilayers at around 30 K [9]. The precise determination of uniaxial strain effects as demonstrated by gigantic uniaxial pressure dependencies reported here is hence mandatory to engineer T_C to the room temperature as a next step towards applications.

In particular due to groundbreaking recent discoveries of long-range magnetic order in bilayers of $Cr_2Ge_2Te_6$ [9] and down to the monolayer in CrI_3 [10], quasi-2D layered vdW materials are at the forefront of research. The layered structure with weak bonding between individual layers makes these materials very attractive for both fundamental research and application-oriented communities. Fundamental research on magnetic vdW materials is focused on the origin and control of their magnetic anisotropy and spin-coupling mechanisms [11,12], whereas research on applications ranges from integration into vdW heterostructures [13,14], vdW-materials-based spintronic devices [15–17], and field effect transistors, e.g., using layered $NiPS_3$ [18], to thermoelectric devices [19].

In bulk $Cr_2Ge_2Te_6$, ferromagnetism evolves at $T_C \simeq 65$ K [20,21]. It crystallizes in the trigonal space group $R\bar{3}$ (No. 148) and belongs to the class of layered vdW transition metal trichalcogenides (TMTCs). The edge-sharing transition metal chalcogenides form a honeycomb network. These honeycomb layers are stacked along the c axis with a vdW gap between adjacent layers (Fig. S1 of the Supplemental Material [22]). A key feature in the layered magnetic vdW materials is magnetic anisotropy, which enables the persistence of long-range magnetic order down to the bilayer or monolayer limit. It originates from the crystallographic lattice, which is connected to the electronic spins via spin-orbit coupling [12,21]. Previous studies investigated the control of magnetic anisotropy in $Cr_2Ge_2Te_6$ by hydrostatic pressure, discussing the possibility of switching the uniaxial anisotropy under pressure from the crystallographic c axis in the unstrained system to an in-plane anisotropy [23,24]. Moreover, spin correlations in $Cr_2Ge_2Te_6$ up to 160 K, i.e., about 2.5 times T_C, were inferred from static magnetic susceptibility and X-band electron spin resonance (ESR) measurements [20,25], and angle-resolved photoemission spectroscopy (ARPES) spectra of $Cr_2Ge_2Te_6$ at 150 K rather suggest a ferromagnetic than a paramagnetic state [26].

These findings motivated us to investigate $Cr_2Ge_2Te_6$ by means of high-resolution capacitance dilatometry to study lattice changes under changing temperature or magnetic field at very high resolution [27]. What is more, in conjunction with specific heat measurements it enables the derivation of the uniaxial pressure dependencies of T_C from thermodynamic relations, providing the means to quantify the magnetoelastic coupling in a material. In contrast to hydrostatic pressure, uniaxial pressure dependencies are otherwise hard to access experimentally for $Cr_2Ge_2Te_6$.

Single crystals of $Cr_2Ge_2Te_6$ have been grown by the self-flux technique and were characterized in detail as reported in Refs. [20,21]. High-resolution dilatometry measurements were performed by means of two three-terminal high-resolution capacitance dilatometers from

*sven.spachmann@kip.uni-heidelberg.de
†s.aswartham@ifw-dresden.de
‡klingeler@kip.uni-heidelberg.de

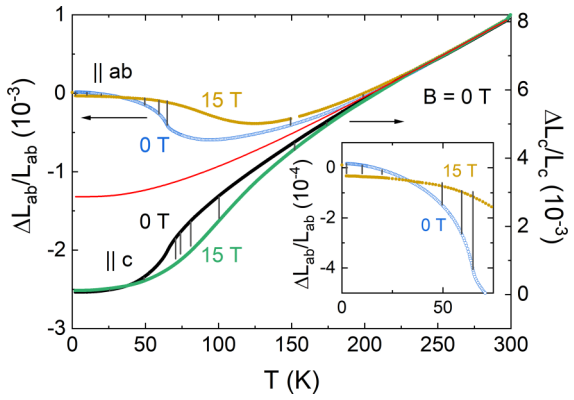

FIG. 1. Thermal expansion at 0 and 15 T with nonmagnetic background estimate. Relative length changes in zero field (black and blue circles) and at $B = 15$ T (green and brown symbols) for $B \parallel ab$ and $B \parallel c$. Left and right ordinates have been shifted and scaled. The red curve shows the estimated phonon background (see the text). Vertical lines indicate the length changes between 0 and 15 T obtained from magnetostriction measurements at selected temperatures. The inset highlights the low-temperature behavior of $\Delta L_{ab}(T)$.

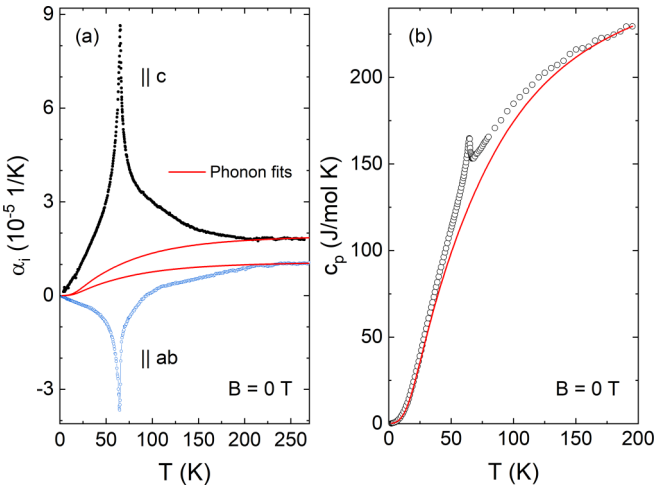

FIG. 2. (a) Thermal expansion coefficients α_i, $i = c, ab$, and (b) specific heat at $B = 0$ T. The red curves show the background fits as explained in the text.

Kuechler Innovative Measurement Technology in a home-built setup placed inside a variable-temperature insert in an Oxford magnet system [27–29]. The capacitance readout was facilitated by Andeen-Hagerling's AH 2550A ultraprecision 1-kHz capacitance bridge [30]. With the dilatometers, the uniaxial thermal expansion $\Delta L_i(T)/L_i$ and the linear thermal expansion coefficients $\alpha_i = 1/L_i \cdot dL_i(T)/dT$ both along the c axis and along the in-plane direction, i.e., $\parallel ab$, were studied at temperatures between 2 and 300 K in zero field and in magnetic fields up to 15 T applied along the direction of the measured length changes. In addition, the field-induced length changes $\Delta L_i(B_i)$ were measured at various fixed temperatures between 2 and 204 K in magnetic fields up to 15 T [31]. The crystals measured in this study were cut to cuboid shapes with lengths of the order of 300 μm along the c axis. In-plane measurements were performed on a crystal with dimensions of 1.3×2.0 mm^2 ($l_{ab} = 1.29$ mm) in the ab plane. Zero-field specific heat was determined in a Physical Property Measurement System (PPMS) from Quantum Design.

Thermal expansion measurements evidence strong magnetoelastic coupling in $Cr_2Ge_2Te_6$ as shown by pronounced kinks in $\Delta L/L$ (Fig. 1) and corresponding peaks in the thermal expansion coefficients at T_C, in zero magnetic field [Fig. 2(a)]. The anomalies signal a continuous phase transition with an increase (decrease) in the in-plane (out-of-plane) lattice parameters at T_C upon cooling. As pressure stabilizes the phase with smaller lattice, this implies negative dependence of T_C on pressure applied within the ab plane whereas pressure applied along the c axis will increase T_C. The anomalies in the thermal expansion data in Fig. 2 are very pronounced at T_C, but extend from the lowest measured temperatures up to at least 200 K, which can easily be seen for the c axis: Phononic contributions to the thermal expansion coefficient are expected to monotonically increase with temperature, whereas α_c decreases until about 200 K, where it reaches a plateau. This behavior suggests a large regime of nonphononic precursory length changes above the long-range ferromagnetic ordering temperature. The precursory length changes are associated with negative in-plane thermal expansion up to nearly 95 K, whereas α_c is positive in the whole temperature regime under study [32].

Applying an external magnetic field of 15 T yields distinct field-induced effects on the length changes (Fig. 1, green and brown symbols). Note that the 15-T data for each axis in Fig. 1 are shifted vertically to coincide at highest temperatures with the respective 0-T data where magnetostriction is vanishing. The field effect at 15 T becomes distinguishable upon cooling below roughly 210 K. Experimentally determined magnetostriction $\Delta L(B)/L(0)$ unambiguously confirms the magnetic field effect [vertical lines in Fig. 1 showing $(L(15\text{ T}) - L(0))/L(0)$ at various temperatures; see also Fig. S5]. In line with this large field effect, the peak in the thermal expansion coefficients shifts to higher temperatures upon application of the magnetic field for both directions, i.e., to 90 K (in plane) and 103 K (c axis), and broadens substantially (Fig. S3). For $B \parallel c$, the data imply shrinking of the c axis at 30 K $\lesssim T \lesssim$ 210 K and only very small magnetostriction outside this temperature regime. In contrast, magnetostriction is positive for $B \parallel ab$ but changes sign at $\sim$37 K (see inset of Fig. 1). The magnetostriction coefficient is given by $\lambda_i = 1/L_i \partial L_i/\partial B = -\partial M/\partial p_i$, where M is the magnetization and p_i is the stress applied along i. This observation implies a sign change of the uniaxial pressure dependence of the magnetization from $\partial M/\partial p_{ab} > 0$ to $\partial M/\partial p_{ab} < 0$ at low temperatures. The c-axis pressure dependence $\partial M/\partial p_c$, on the other hand, is very small at lowest temperatures.

In order to estimate nonphononic contributions to the thermal expansion of $Cr_2Ge_2Te_6$, an estimate of the phononic contributions is necessary [33]. In general, the phononic contribution to the linear thermal expansion coefficient α_i is related to the specific heat of a phonon mode j, $c_{ph,j}$ (in J mol^{-1} K^{-1}), by the compressibility κ (in GPa^{-1}) and a

Grüneisen parameter $\gamma_{i,j}$ (dimensionless) as

$$\alpha_{i,ph}(T) = \frac{\kappa}{3V_m} \cdot \sum_j \gamma_{i,j} \cdot c_{ph,j}(T), \quad (1)$$

1.67×10^{-4} m^3/mol is the molar volume for $Cr_2Ge_2Te_6$, calculated from the unit cell volume $V_0 = 811$ Å^3 [33] and $M_{mol} = 1014.87$ g/mol with three formula units per unit cell. The specific heat of a phonon mode can be modeled in different ways. Often a Debye approximation (for formula, see Supplemental Material), which assumes a linear dispersion of a phonon branch, is used to model acoustic phonons and low-temperature behavior, whereas an Einstein approximation is applied when optical phonons dominate. We tried different combinations of Debye and Einstein modes. The best fit to the specific heat data [Fig. 2(b)] was achieved by (1) optimizing for a total magnetic entropy in line with a spin-$\frac{3}{2}$ system, $S_{mag} \approx S_{mag,theor} = 2R\ln(4)$ (with 2 moles of Cr atoms per mole of $Cr_2Ge_2Te_6$and R being the molar gas constant), as well as (2) assuming that the peak shape of $c_{p,mag}$ should resemble that of the thermal expansion coefficient and (3) assuming that the magnetic entropy should vanish around 200 K as indicated by the plateau in α_c [Fig. 2(a)] as explained above. With these assumptions we obtained the best fit for a combination of only two Debye modes with Debye temperatures $\Theta_{D,1} = 150$ K and $\Theta_{D,2} = 410$ K and a Sommerfeld coefficient $\gamma_{el} = 60$ mJ mol^{-1} K^{-2} (obtained from the low-temperature behavior; see Supplemental Material). The magnetic specific heat (Fig. 3, black squares) results from subtracting the phonon fit from c_p. The related magnetic entropy shows that only 56% of the full magnetic entropy is contained below T_C. Phonon fits to the thermal expansion coefficients [Fig. 2(a)] are obtained according to Eq. (1) by multiplying the phononic specific heat by a constant, the effective Grüneisen parameter $\gamma_{i,eff} = \kappa\gamma_i/(3V_m)$, to fit the high-temperature behavior of α_i. With this approach we assume a constant bulk compressibility, $\kappa(T) = \text{const}$, as well as a constant Grüneisen parameter which is the same for both Debye modes, $\gamma_{i,1} = \gamma_{i,2} = \gamma_i$, $i = c, ab$. This results in $\gamma_{c,eff} = 8.05(10) \times 10^{-8}$ mol/J and $\gamma_{ab,eff} = 4.5(1) \times 10^{-8}$ mol/J. Bulk compressibilities for $Cr_2Ge_2Te_6$ have not been determined experimentally, but a bulk modulus $B = 1/\kappa = 14$ GPa has been reported from density functional theory (DFT) calculations [34], i.e., $\kappa = 0.071$ GPa^{-1}. Applying this result from calculations yields an estimate of the Grüneisen parameters $\gamma_c = 0.56$ and $\gamma_{ab} = 0.32$. The estimated nonmagnetic background in Fig. 1 is obtained by integration of these fits with respect to temperature.

As seen in Figs. 1 and 2, above 205 K the thermal expansion is described very well by the phonon background. Upon cooling below 205 K, in contrast, nonphononic thermal expansion evolves which is anisotropic in nature. We attribute the nonphonon behavior to magnetic degrees of freedom. A comparison of these magnetic contributions to the specific heat and thermal expansion reveals that they scale over the full range from 0 to 200 K except at the Curie temperature (Fig. 3; see also Fig. S4). This scaling implies the presence of only one dominant energy scale [35,36]. While the c axis shows a nearly perfect scaling from 200 to 80 K and good scaling below 64 K, minor deviations can be seen

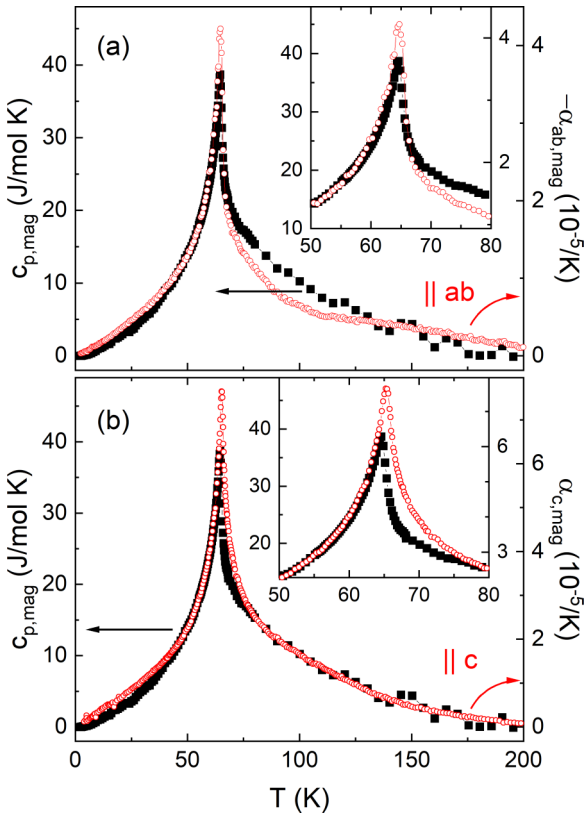

FIG. 3. Grüneisen scaling of thermal expansion and specific heat. Comparison of $\alpha_{i,mag}$ (red open symbols) and $c_{p,mag}$ (black closed symbols) at $B = 0$ T for the in-plane direction (a) and the c axis (b) yielding the magnetic Grüneisen parameters $\gamma_{ab,mag} = 4.2-7.8$ and $\gamma_{c,mag} = 11.3$ (see text).

for the *ab* plane, especially between 70 and 130 K. The effective magnetic Grüneisen parameter for the c axis is $\gamma_{c,mag,eff} = 1.6 \times 10^{-6}$ mol/J, and $\gamma_{ab,mag,eff}$ varies from -6×10^{-7} to -1.1×10^{-6} mol/J between 120 and 30 K. With $\kappa = 0.071$ GPa^{-1} as before this yields large magnetic Grüneisen factors $\gamma_{c,mag} = 11.3$ and $\gamma_{ab,mag} = 4.2-7.8$. These values are of the same magnitude as other magnetic Grüneisen factors, e.g., $\gamma_{mag} \approx -18$ for α-Mn [37]. A part of the deviations around T_C stems from the fact that the specific heat was measured by a relaxation method and thus averages over a temperature range, whereas the thermal expansion data are measured closer to thermal equilibrium, with a warming rate of 0.3 K/min. Effects of uniaxial pressure and strain, as well as domain formation, presumably contribute further to the deviations. Furthermore, the bulk modulus may change around T_C and lead to additional differences between thermal expansion and specific heat.

On top of the analysis of Grüneisen scaling, the uniaxial pressure dependence of the ordering temperature can be determined by the method suggested by Souza *et al.* for continuous phase transitions exhibiting critical behavior [38]. This method has been applied to a number of materials and was verified in comparison to experimental pressure dependencies by studies on $LaMnO_3$ and $CaMnO_3$ [39,40], as well as Na_xCoO_2 [41–43]. The pressure dependence is obtained by subtracting from the specific heat a constant offset as well as

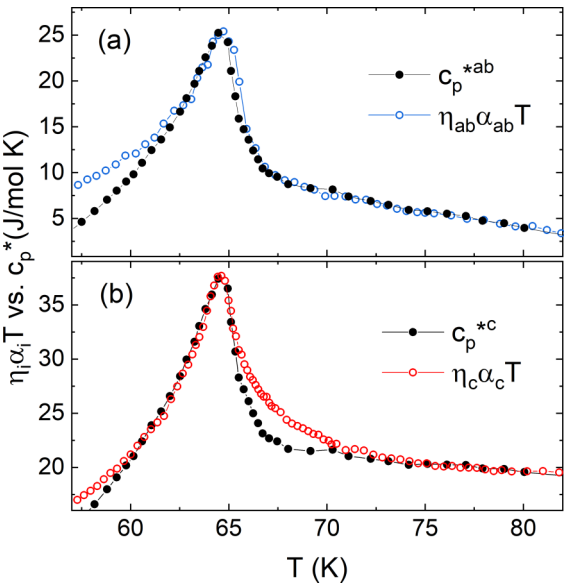

FIG. 4. Scaling of the specific heat and thermal expansion coefficients in order to obtain the uniaxial pressure dependence according to Ref. [38]. The thermal expansion coefficients were rescaled by (a) $\eta_{ab} = -10\,700$ J mol^{-1} K^{-1} and (b) $\eta_c = 6750$ J mol^{-1} K^{-1}. $\eta_c\alpha_c$T was shifted by -0.8 K so that its peak position overlaps with the peak position of $c_p^{*,c}$. Background subtractions with $a = 48$ J mol^{-1} K^{-1}, $b = 1.42$ J mol^{-1} K^{-2} ($a = 50$ J mol^{-1} K^{-1}, $b = 1.2$ J mol^{-1} K^{-2}) were performed on c_p to obtain $c_p^{*,ab}$ ($c_p^{*,c}$).

a linear term to obtain

$$c_p^* \equiv c_p - a - bT \tag{2}$$

and subsequently superimposing c_p^* with the rescaled thermal expansion coefficients $\eta_i\alpha_i T$ (in J mol^{-1} K^{-1}) in a small-temperature regime around T_C [44]. The uniaxial pressure dependence is then given by

$$\frac{dT_C}{dp_i} \equiv \left(\frac{dp_i}{dT}\right)_C^{-1} = \frac{\eta_i\alpha_i T}{c_p^*}. \tag{3}$$

Analyzing our data this way we obtain scaling factors $\eta_c = 6750(400)$ J mol^{-1} K^{-1} and $\eta_{ab} = -10700(600)$ J mol^{-1} K^{-1} (Fig. 4). From $\partial T_C/\partial p_i = \frac{V_m}{\eta_i}$ we then obtain $\partial T_C/\partial p_c = 24.7(1.8)$ K/GPa and $\partial T_C/\partial p_{ab} = -15.6(1.1)$ K/GPa. Assuming that the hydrostatic pressure dependence can be calculated by superimposing the uniaxial ones in the three main directions yields an estimate of $dT_C/dp_{p\to 0} = 2\,\partial T_C/\partial p_{ab} + \partial T_C/\partial p_c = -6.5(8)$ K/GPa.

Our observation of nonphononic lattice changes up to 200 K visible in the thermal expansion (Fig. 2) confirms the presence of short-range magnetic order far above T_C and provides a macroscopic measurement of high-temperature magnetostructural correlations in $Cr_2Ge_2Te_6$. This observation strongly supports the expected quasi-2D nature of magnetism in $Cr_2Ge_2Te_6$ and suggests low-dimensional exchange interactions [45,46]. Deviations from purely paramagnetic behavior up to around 150 K were previously observed in the static susceptibility [25], in X-band ESR spectra [20], and in ARPES [26]. Moreover, temperature-dependent Raman spectra of $Cr_2Ge_2Te_6$ show a mode around 122 cm^{-1} broadening strongly upon cooling between 200 and 250 K [47]. Direct investigation of magnetic correlations on the isostructural ferromagnet $Cr_2Si_2Te_6$, which also possesses uniaxial c-axis magnetic anisotropy, revealed static and dynamic magnetic in-plane correlations at least up to 300 K, almost ten times the long-range ordering temperature $T_C = 33$ K [46].

Low-dimensional high-temperature correlations are especially of interest from a fundamental perspective. The effects of pressure on the critical temperatures and other physical properties in magnetic vdW compounds, on the other hand, are a field of intense research with an eye on precisely tuning material properties for technological applications. Accordingly, the effects of stress and strain on $Cr_2Ge_2Te_6$ [24,47,48] and related materials [49–56] have been intensively studied both experimentally and numerically. Previous experimental studies on $Cr_2Ge_2Te_6$ were restricted to hydrostatic pressure p_h, the effect of which on the layered structure is not *a priori* clear and is supposed to mainly modify the interlayer structure [57]. Hydrostatic pressure is found to decrease T_C, the response being stronger for small applied pressure than for larger pressures. In the ranges from 0 to 0.25 GPa [47] and from 0 to 0.1 GPa [48] a drop in T_C of about -14 K/GPa was observed, compared with about -4 K/GPa for pressures of 1 GPa and above [24], which is in good agreement with $dT_C/dp_{p\to 0} = -6.5(8)$ K/GPa derived from our thermal expansion and specific heat data. A more recent study found smaller changes of about -12 K between 0 and 4.5 GPa, i.e., a drop by about 2.7 K/GPa [58]. The changes in T_C under hydrostatic pressure have been ascribed to the interplay of a decrease in Cr–Cr and Cr–Te bond lengths and an increase in Cr–Te–Cr bond angle away from 90° upon increasing p_h, i.e., the complex competition between antiferromagnetic (AFM) direct exchange between Cr ions and superexchange mediated by the Te ions [24,49,59]. In this respect, our observation that (uniaxial) in-plane pressure yields a drastic decrease in T_C is particularly relevant as it suggests that the observed dT_C/dp_h is much more moderate due to the out-of-plane pressure components. This conclusion is supported by recent numerical studies of in-plane and out-of-plane exchange couplings, J_{in} and J_{out}, which show a strong increase in J_{out} upon application of hydrostatic pressure, with an initial effect of about 35%/GPa, whereas J_{in} was found to decrease by about -10%/GPa [48]. The data presented here are also consistent with recent density functional theory calculations on $Cr_2Si_2Te_6$ where a strong enhancement of T_C by in-plane biaxial tensile strain was found [49].

Our study *experimentally* evidences and *quantifies* by thermodynamic relations very large uniaxial pressure effects in $Cr_2Ge_2Te_6$. These large effects strongly underline the feasibility of using the material for potential applications, as tailoring of the transition temperature is made possible by applying moderate in-plane tensile strain. Especially, enhancing T_C with the goal of room-temperature applications is essential for actual devices, e.g., for sensing, data storage, or computing. The practical feasibility of such T_C enhancement in $Cr_2Ge_2Te_6$ has been shown by Wang *et al.*, who managed to enhance T_C to 208 K by electrochemical intercalation of organic molecules into the van der Waals gap [60]. Adding to this result the large in-plane pressure dependence which we

report here, in particular, suggests an exceptional feasibility of using $Cr_2Ge_2Te_6$ for strain-tailoring ferromagnetism.

Although there are quite a number of theoretical studies on the effects of strain and stress on $Cr_2Ge_2Te_6$ and other magnetic vdW materials as mentioned above, experimental results for the uniaxial pressure dependencies of these materials are very rare. To the best of our knowledge, such measurements only exist for CrI_3 [61] and α-$RuCl_3$ [62]. CrI_3 also exhibits ferromagnetic layers but shows a much smaller uniaxial pressure dependence of only $\partial T_C/\partial p_{ab} = -0.4(1)$ K/GPa [61], i.e., of the same sign, but drastically, by more than one order of magnitude, smaller than in $Cr_2Ge_2Te_6$. In contrast, the Kitaev spin liquid candidate α-$RuCl_3$ exhibits uniaxial pressure dependencies for its different transitions of $\partial T_N/\partial p_a = -3.5$ K/GPa to $\partial T_N/\partial p_c = -14.5$ K/GPa. These values are much larger than those found for CrI_3 and yet still about two to four times smaller than what we report here for $Cr_2Ge_2Te_6$. Note that this drastic difference is not reflected in the initial hydrostatic pressure dependencies of either CrI_3 or α-$RuCl_3$, which are reported to be of similar size to that in $Cr_2Ge_2Te_6$, $dT_C/dp = 12$ K/GPa [63] and $dT_N/dp \approx -13$ to -24 K/GPa [62], respectively. In order to further emphasize the size of pressure dependencies found in $Cr_2Ge_2Te_6$, it is instructive to compare our results also with hydrostatic pressure dependencies of other quasi-2D magnetic materials with a honeycomb lattice, such as VI_3 [64], $FePS_3$ [65], $Na_3Ni_2SbO_6$ [29], and β-Li_2IrO_3 [66]. These materials exhibit a large range of pressure dependencies differing by two orders of magnitude. Very small hydrostatic pressure dependencies have been reported for the vdW compound VI_3 [64,67], with $dT_C/dp \approx 0$ at small pressures, and for $Na_3Ni_2SbO_6$, with $dT_N/dp = -0.05$ K/GPa [29]. Dilatometric studies of the Kitaev hyperhoneycomb iridate β-Li_2IrO_3 yield larger values of $dT_N/dp = 0.7$ K/GPa [66]. Finally, a hydrostatic pressure dependence of $dT_N/dp = 7.7$ K/GPa is observed in the vdW antiferromagnet $FePS_3$ [65].

In conclusion, the quasi-2D layered van der Waals compound $Cr_2Ge_2Te_6$ shows strong magnetoelastic coupling giving rise to large uniaxial pressure dependencies of T_C. These results confirm that moderate in-plane tensile strain is sufficient to strongly enhance the long-range ferromagnetic ordering temperature. Our high-resolution thermal expansion data in addition unambiguously prove short-range magnetic order up to 200 K. The large uniaxial pressure effects and quasi-2D nature of magnetism in $Cr_2Ge_2Te_6$ present an intriguing playground for $Cr_2Ge_2Te_6$-based technological applications, bringing into reach room-temperature ferromagnetism in 2D materials.

We acknowledge financial support by BMBF via the project SpinFun (13XP5088) and by Deutsche Forschungsgemeinschaft (DFG) under Germany's Excellence Strategy EXC2181/1-390900948 (the Heidelberg STRUCTURES Excellence Cluster) and through Projects No. KL 1824/13-1 (R.K.) and No. AS 523/4-1 (S.A.). B.B. acknowledges the Würzburg-Dresden Cluster of Excellence on Complexity and Topology in Quantum Matter - ct.qmat (EXC 2147, Project No. 390858490).

[1] S. Chen, A. Sood, E. Pop, K. E. Goodson, and D. Donadio, Strongly tunable anisotropic thermal transport in MoS_2 by strain and lithium intercalation: First-principles calculations, 2D Mater. **6**, 025033 (2019).

[2] Z. Peng, X. Chen, Y. Fan, D. J. Srolovitz, and D. Lei, Strain engineering of 2D semiconductors and graphene: From strain fields to band-structure tuning and photonic applications, Light Sci. Appl. **9**, 190 (2020).

[3] Y. Chen, Y. Lei, Y. Li, Y. Yu, J. Cai, M.-H. Chiu, R. Rao, Y. Gu, C. Wang, W. Choi, H. Hu, C. Wang, Y. Li, J. Song, J. Zhang, B. Qi, M. Lin, Z. Zhang, A. E. Islam, B. Maruyama *et al.*, Strain engineering and epitaxial stabilization of halide perovskites, Nature (London) **577**, 209 (2020).

[4] G. Tsutsui, S. Mochizuki, N. Loubet, S. W. Bedell, and D. K. Sadana, Strain engineering in functional materials, AIP Adv. **9**, 030701 (2019).

[5] J. Cenker, S. Sivakumar, K. Xie, A. Miller, P. Thijssen, Z. Liu, A. Dismukes, J. Fonseca, E. Anderson, X. Zhu, X. Roy, D. Xiao, J.-H. Chu, T. Cao, and X. Xu, Reversible strain-induced magnetic phase transition in a van der Waals magnet, Nat. Nanotechnol. **17**, 256 (2022).

[6] D. G. Schlom, L.-Q. Chen, C. J. Fennie, V. Gopalan, D. A. Muller, X. Pan, R. Ramesh, and R. Uecker, Elastic strain engineering of ferroic oxides, MRS Bull. **39**, 118 (2014).

[7] T. Wang, A. Prakash, Y. Dong, T. Truttmann, A. Bucsek, R. James, D. D. Fong, J.-W. Kim, P. J. Ryan, H. Zhou, T. Birol, and B. Jalan, Engineering $SrSnO_3$ phases and electron mobility at room temperature using epitaxial strain, ACS Appl. Mater. Interfaces **10**, 43802 (2018).

[8] P. Homm, M. Menghini, J. W. Seo, S. Peters, and J.-P. Locquet, Room temperature Mott metal-insulator transition in V_2O_3 compounds induced via strain-engineering, APL Mater. **9**, 021116 (2021).

[9] C. Gong, L. Li, Z. Li, H. Ji, A. Stern, Y. Xia, T. Cao, W. Bao, C. Wang, Y. Wang, Z. Q. Qiu, R. J. Cava, S. G. Louie, J. Xia, and X. Zhang, Discovery of intrinsic ferromagnetism in two-dimensional van der Waals crystals, Nature (London) **546**, 265 (2017).

[10] B. Huang, G. Clark, E. Navarro-Moratalla, D. R. Klein, R. Cheng, K. L. Seyler, D. Zhong, E. Schmidgall, M. A. McGuire, D. H. Cobden, W. Yao, D. Xiao, P. Jarillo-Herrero, and X. Xu, Layer-dependent ferromagnetism in a van der Waals crystal down to the monolayer limit, Nature (London) **546**, 270 (2017).

[11] X. Zhang, Y. Zhao, Q. Song, S. Jia, J. Shi, and W. Han, Magnetic anisotropy of the single-crystalline ferromagnetic insulator $Cr_2Ge_2Te_6$, Jpn. J. Appl. Phys. **55**, 033001 (2016).

[12] D.-H. Kim, K. Kim, K.-T. Ko, J. H. Seo, J. S. Kim, T.-H. Jang, Y. Kim, J.-Y. Kim, S.-W. Cheong, and J.-H. Park, Giant Magnetic Anisotropy Induced by Ligand *LS* Coupling in Layered Cr Compounds, Phys. Rev. Lett. **122**, 207201 (2019).

[13] H. Idzuchi, A. E. Llacsahuanga Allcca, X. C. Pan, K. Tanigaki, and Y. P. Chen, Increased Curie temperature and enhanced

perpendicular magneto anisotropy of $Cr_2Ge_2Te_6$/NiO heterostructures, Appl. Phys. Lett. **115**, 232403 (2019).

[14] M. Blei, J. L. Lado, Q. Song, D. Dey, O. Erten, V. Pardo, R. Comin, S. Tongay, and A. S. Botana, Synthesis, engineering, and theory of 2D van der Waals magnets, Appl. Phys. Rev. **8**, 021301 (2021).

[15] D. Zhong, K. L. Seyler, X. Linpeng, R. Cheng, N. Sivadas, B. Huang, E. Schmidgall, T. Taniguchi, K. Watanabe, M. A. McGuire, W. Yao, D. Xiao, K.-M. C. Fu, and X. Xu, Van der Waals engineering of ferromagnetic semiconductor heterostructures for spin and valleytronics, Sci. Adv. **3**, e1603113 (2017).

[16] Z. Wang, I. Gutiérrez-Lezama, N. Ubrig, M. Kroner, M. Gibertini, T. Taniguchi, K. Watanabe, A. Imamoğlu, E. Giannini, and A. F. Morpurgo, Very large tunneling magnetoresistance in layered magnetic semiconductor CrI_3, Nat. Commun. **9**, 2516 (2018).

[17] M. Alghamdi, M. Lohmann, J. Li, P. R. Jothi, Q. Shao, M. Aldosary, T. Su, B. P. T. Fokwa, and J. Shi, Highly Efficient spin-orbit torque and switching of layered ferromagnet Fe_3GeTe_2, Nano Lett. **19**, 4400 (2019).

[18] R. N. Jenjeti, R. Kumar, M. P. Austeria, and S. Sampath, Field effect transistor based on layered $NiPS_3$, Sci. Rep. **8**, 8586 (2018).

[19] X. Tang, D. Fan, K. Peng, D. Yang, L. Guo, X. Lu, J. Dai, G. Wang, H. Liu, and X. Zhou, Dopant induced impurity bands and carrier concentration control for thermoelectric enhancement in p-type $Cr_2Ge_2Te_6$, Chem. Mater. **29**, 7401 (2017).

[20] J. Zeisner, A. Alfonsov, S. Selter, S. Aswartham, M. P. Ghimire, M. Richter, J. van den Brink, B. Büchner, and V. Kataev, Magnetic anisotropy and spin-polarized two-dimensional electron gas in the van der Waals ferromagnet $Cr_2Ge_2Te_6$, Phys. Rev. B **99**, 165109 (2019).

[21] S. Selter, G. Bastien, A. U. B. Wolter, S. Aswartham, and B. Büchner, Magnetic anisotropy and low-field magnetic phase diagram of the quasi-two-dimensional ferromagnet $Cr_2Ge_2Te_6$, Phys. Rev. B **101**, 014440 (2020).

[22] See Supplemental Material at http://link.aps.org/supplemental/10.1103/PhysRevResearch.4.L022040 for details.

[23] Z. Lin, M. Lohmann, Z. A. Ali, C. Tang, J. Li, W. Xing, J. Zhong, S. Jia, W. Han, S. Coh, W. Beyermann, and J. Shi, Pressure-induced spin reorientation transition in layered ferromagnetic insulator $Cr_2Ge_2Te_6$, Phys. Rev. Materials **2**, 051004(R) (2018).

[24] T. Sakurai, B. Rubrecht, L. T. Corredor, R. Takehara, M. Yasutani, J. Zeisner, A. Alfonsov, S. Selter, S. Aswartham, A. U. B. Wolter, B. Büchner, H. Ohta, and V. Kataev, Pressure control of the magnetic anisotropy of the quasi-two-dimensional van der Waals ferromagnet $Cr_2Ge_2Te_6$, Phys. Rev. B **103**, 024404 (2021).

[25] Y. Sun, W. Tong, and X. Luo, Possible magnetic correlation above the ferromagnetic phase transition temperature in $Cr_2Ge_2Te_6$, Phys. Chem. Chem. Phys. **21**, 25220 (2019).

[26] M. Suzuki, B. Gao, K. Koshiishi, S. Nakata, K. Hagiwara, C. Lin, Y. X. Wan, H. Kumigashira, K. Ono, S. Kang, S. Kang, J. Yu, M. Kobayashi, S.-W. Cheong, and A. Fujimori, Coulomb-interaction effect on the two-dimensional electronic structure of the van der Waals ferromagnet $Cr_2Ge_2Te_6$, Phys. Rev. B **99**, 161401(R) (2019).

[27] R. Küchler, T. Bauer, M. Brando, and F. Steglich, A compact and miniaturized high resolution capacitance dilatometer for measuring thermal expansion and magnetostriction, Rev. Sci. Instrum. **83**, 095102 (2012).

[28] R. Küchler, A. Wörl, P. Gegenwart, M. Berben, B. Bryant, and S. Wiedmann, The world's smallest capacitive dilatometer, for high-resolution thermal expansion and magnetostriction in high magnetic fields, Rev. Sci. Instrum. **88**, 083903 (2017).

[29] J. Werner, W. Hergett, M. Gertig, J. Park, C. Koo, and R. Klingeler, Anisotropy-governed competition of magnetic phases in the honeycomb quantum magnet $Na_3Ni_2SbO_6$ studied by dilatometry and high-frequency ESR, Phys. Rev. B **95**, 214414 (2017).

[30] Andeen-Hagerling Inc., AH 2550A 1 kHz Ultra-Precision Capacitance Bridge, http://www.andeen-hagerling.com/ah2550a.htm.

[31] S. Spachmann, Thermal expansion and magnetostriction of layered correlated electron systems, Ph.D. thesis, Heidelberg University, 2021.

[32] Due to the softness of the material, in-plane sample mounting is very susceptible to pressure inevitably applied in the capacitance dilatometer, and in-plane length changes display larger error bars than out-of-plane data. In particular, different mounting of the sample yields a somewhat smaller anomaly in α_{ab} at T_C.

[33] A phonon background correction using the nonmagnetic analog $In_2Ge_2Te_6$ was unsuccessful; see Supplemental Material.

[34] K. Persson, Materials data on $CrGeTe_3$ (SG:148), Materials Project, 2016, https://materialsproject.org/materials/mp-541449/.

[35] P. Gegenwart, Grüneisen parameter studies on heavy fermion quantum criticality, Rep. Prog. Phys. **79**, 114502 (2016).

[36] R. Klingeler, J. Geck, S. Arumugam, N. Tristan, P. Reutler, B. Büchner, L. Pinsard-Gaudart, and A. Revcolevschi, Pressure-induced melting of the orbital polaron lattice in $La_{1-x}Sr_xMnO_3$, Phys. Rev. B **73**, 214432 (2006).

[37] B. D. White, R. K. Bollinger, and J. J. Neumeier, Thermal expansion and thermodynamic characterization of antiferromagnetic phase transition in elemental α-Mn, Phys. Status Solidi B **252**, 198 (2015).

[38] J. A. Souza, Y.-K. Yu, J. J. Neumeier, H. Terashita, and R. F. Jardim, Method for Analyzing Second-Order Phase Transitions: Application to the Ferromagnetic Transition of a Polaronic System, Phys. Rev. Lett. **94**, 207209 (2005).

[39] J.-S. Zhou and J. B. Goodenough, Exchange interactions in the perovskites $Ca_{1-x}Sr_xMnO_3$ and $RMnO_3$(R = La, Pr, Sm), Phys. Rev. B **68**, 054403 (2003).

[40] J. A. Souza, J. J. Neumeier, B. D. White, and Y.-K. Yu, Analysis of the critical behavior associated with the antiferromagnetic transitions of $LaMnO_3$ and $CaMnO_3$, Phys. Rev. B **81**, 172410 (2010).

[41] Y. V. Sushko, O. B. Korneta, S. O. Leontsev, R. Jin, B. C. Sales, and D. Mandrus, Pressure dependence of magnetic and superconducting transitions in sodium cobalt oxides Na_xCoO_2, arXiv:cond-mat/0509308.

[42] J. Wooldridge, D. M. Paul, G. Balakrishnan, and M. R. Lees, The magnetic field and pressure dependence of the magnetic ordering transition in Na_xCoO_2 ($0.6 \leqslant x \leqslant 0.72$), J. Phys.: Condens. Matter **18**, 4731 (2006).

[43] C. A. M. dos Santos, J. J. Neumeier, Y.-K. Yu, R. K. Bollinger, R. Jin, D. Mandrus, and B. C. Sales, Thermodynamic nature of

the antiferromagnetic transition in Na_xCoO_2, Phys. Rev. B **74**, 132402 (2006).

[44] Note that the temperature for α_c was rescaled by subtracting 0.8 K, because the peak value is reached at 64.7 K for the specific heat data and α_{ab}, whereas it is reached at 65.5 K for α_c.

[45] S. Calder, A. V. Haglund, A. I. Kolesnikov, and D. Mandrus, Magnetic exchange interactions in the van der Waals layered antiferromagnet $MnPSe_3$, Phys. Rev. B **103**, 024414 (2021).

[46] T. J. Williams, A. A. Aczel, M. D. Lumsden, S. E. Nagler, M. B. Stone, J.-Q. Yan, and D. Mandrus, Magnetic correlations in the quasi-two-dimensional semiconducting ferromagnet $CrSiTe_3$, Phys. Rev. B **92**, 144404 (2015).

[47] Y. Sun, R. C. Xiao, G. T. Lin, R. R. Zhang, L. S. Ling, Z. W. Ma, X. Luo, W. J. Lu, Y. P. Sun, and Z. G. Sheng, Effects of hydrostatic pressure on spin-lattice coupling in two-dimensional ferromagnetic $Cr_2Ge_2Te_6$, Appl. Phys. Lett. **112**, 072409 (2018).

[48] A. O. Fumega, S. Blanco-Canosa, H. Babu-Vasili, P. Gargiani, H. Li, J.-S. Zhou, F. Rivadulla, and V. Pardo, Electronic structure and magnetic exchange interactions of Cr-based van der Waals ferromagnets. a comparative study between $CrBr_3$ and $Cr_2Ge_2Te_6$, J. Mater. Chem. C **8**, 13582 (2020).

[49] X. Chen, J. Qi, and D. Shi, Strain-engineering of magnetic coupling in two-dimensional magnetic semiconductor $CrSiTe_3$: Competition of direct exchange interaction and superexchange interaction, Phys. Lett. A **379**, 60 (2015).

[50] X. Zhao, Z. Ding, J. Chen, J. Dan, S. M. Poh, W. Fu, S. J. Pennycook, W. Zhou, and K. P. Loh, Strain modulation by van der Waals coupling in bilayer transition metal dichalcogenide, ACS Nano **12**, 1940 (2018).

[51] S. Huang, G. Zhang, F. Fan, C. Song, F. Wang, Q. Xing, C. Wang, H. Wu, and H. Yan, Strain-tunable van der Waals interactions in few-layer black phosphorus, Nat. Commun. **10**, 2447 (2019).

[52] A. M. León, J. W. González, J. Mejía-López, F. Crasto de Lima, and E. Suárez Morell, Strain-induced phase transition in CrI_3 bilayers, 2D Mater. **7**, 035008 (2020).

[53] Y. Wang, C. Wang, S.-J. Liang, Z. Ma, K. Xu, X. Liu, L. Zhang, A. S. Admasu, S.-W. Cheong, L. Wang, M. Chen, Z. Liu, B. Cheng, W. Ji, and F. Miao, Strain-sensitive magnetization reversal of a van der Waals magnet, Adv. Mater. (Weinheim) **32**, 2004533 (2020).

[54] F. Xue, Z. Wang, Y. Hou, L. Gu, and R. Wu, Control of magnetic properties of $MnBi_2Te_4$ using a van der Waals ferroelectric II I_2-VI_3 film and biaxial strain, Phys. Rev. B **101**, 184426 (2020).

[55] Z. Zhang, J.-Y. You, B. Gu, and G. Su, Emergent magnetic states due to stacking and strain in the van der Waals magnetic trilayer CrI_3, Phys. Rev. B **104**, 174433 (2021).

[56] M. Zhu, Y. You, G. Xu, J. Tang, Y. Gong, and F. Xu, Strain modulation of magnetic coupling in the metallic van der Waals magnet Fe_3GeTe_2, Intermetallics **131**, 107085 (2021).

[57] T. Li, S. Jiang, N. Sivadas, Z. Wang, Y. Xu, D. Weber, J. E. Goldberger, K. Watanabe, T. Taniguchi, C. J. Fennie, K. Fai Mak, and J. Shan, Pressure-controlled interlayer magnetism in atomically thin CrI_3, Nat. Mater. **18**, 1303 (2019).

[58] D. Bhoi, J. Gouchi, N. Hiraoka, Y. Zhang, N. Ogita, T. Hasegawa, K. Kitagawa, H. Takagi, K. H. Kim, and Y. Uwatoko, Nearly Room-Temperature Ferromagnetism in a Pressure-Induced Correlated Metallic State of the van der Waals Insulator $CrGeTe_3$, Phys. Rev. Lett. **127**, 217203 (2021).

[59] J. B. Goodenough, *Magnetism and the Chemical Bond* (Interscience, New York, 1963).

[60] N. Wang, H. Tang, M. Shi, H. Zhang, W. Zhuo, D. Liu, F. Meng, L. Ma, J. Ying, L. Zou, Z. Sun, and X. Chen, Transition from ferromagnetic semiconductor to ferromagnetic metal with enhanced Curie temperature in $Cr_2Ge_2Te_6$ via organic ion intercalation, J. Am. Chem. Soc. **141**, 17166 (2019).

[61] J. Arneth, M. Jonak, S. Spachmann, M. Abdel-Hafiez, Y. O. Kvashnin, and R. Klingeler, Uniaxial pressure effects in the two-dimensional van der Waals ferromagnet CrI_3, Phys. Rev. B **105**, L060404 (2022).

[62] M. He, X. Wang, L. Wang, F. Hardy, T. Wolf, P. Adelmann, T. Brückel, Y. Su, and C. Meingast, Uniaxial and hydrostatic pressure effects in α–$RuCl_3$ single crystals via thermal-expansion measurements, J. Phys.: Condens. Matter **30**, 385702 (2018).

[63] S. Mondal, M. Kannan, M. Das, L. Govindaraj, R. Singha, B. Satpati, S. Arumugam, and P. Mandal, Effect of hydrostatic pressure on ferromagnetism in two-dimensional CrI_3, Phys. Rev. B **99**, 180407(R) (2019).

[64] J. Valenta, M. Kratochvílová, M. Míšek, K. Carva, J. Kaštil, P. Doležal, P. Opletal, P. Čermák, P. Proschek, K. Uhlířová, J. Prchal, M. J. Coak, S. Son, J.-G. Park, and V. Sechovský, Pressure-induced large increase of Curie temperature of the van der Waals ferromagnet VI_3, Phys. Rev. B **103**, 054424 (2021).

[65] M. J. Coak, D. M. Jarvis, H. Hamidov, A. R. Wildes, J. A. M. Paddison, C. Liu, C. R. S. Haines, N. T. Dang, S. E. Kichanov, B. N. Savenko, S. Lee, M. Kratochvílová, S. Klotz, T. C. Hansen, D. P. Kozlenko, J.-G. Park, and S. S. Saxena, Emergent Magnetic Phases in Pressure-Tuned van der Waals Antiferromagnet $FePS_3$, Phys. Rev. X **11**, 011024 (2021).

[66] M. Majumder, R. S. Manna, G. Simutis, J. C. Orain, T. Dey, F. Freund, A. Jesche, R. Khasanov, P. K. Biswas, E. Bykova, N. Dubrovinskaia, L. S. Dubrovinsky, R. Yadav, L. Hozoi, S. Nishimoto, A. A. Tsirlin, and P. Gegenwart, Breakdown of Magnetic Order in the Pressurized Kitaev Iridate β–Li_2IrO_3, Phys. Rev. Lett. **120**, 237202 (2018).

[67] S. Son, M. J. Coak, N. Lee, J. Kim, T. Y. Kim, H. Hamidov, H. Cho, C. Liu, D. M. Jarvis, P. A. C. Brown, J. H. Kim, C.-H. Park, D. I. Khomskii, S. S. Saxena, and J.-G. Park, Bulk properties of the van der Waals hard ferromagnet VI_3, Phys. Rev. B **99**, 041402(R) (2019).